Article

Chinese Science Bulletin

Atmospheric Science

August 2010 Vol.55 No.22: 2458–2468
doi: 10.1007/s11434-010-3098-3

Impacts of Atlantic sea surface temperature anomalies on Indo-East Asian summer monsoon-ENSO relationship

RONG XinYao[1*], ZHANG RenHe[1] & LI Tim[2]

[1] *Chinese Academy of Meteorological Sciences, Beijing 100086, China;*
[2] *International Pacific Research Center and Department of Meteorology, University of Hawaii at Manoa, Honolulu HI 96822, USA*

Received September 7, 2009; accepted November 22, 2009

In this study, the effect of the tropical North Atlantic (TNA) sea surface temperature (SST) variation in inducing the circulation anomaly in the Indo-East Asian monsoon (IEAM) region is investigated through the observational analysis and numerical modeling. The observational analysis shows that the TNA summer SST is positively correlated with the preceding winter Niño3 SST and is simultaneously correlated with the circulation in the IEAM region. The simultaneous circulation pattern resembles that of the ENSO-decaying summer. The positive correlation between the TNA SST and the Niño3 region SST is primarily ascribed to the surface latent heat flux and short wave radiation anomalies induced by the ENSO teleconnection. Coupled general circulation model experiments show that, while including the air-sea coupling in the Atlantic, the model can reproduce the main features of the IEAM circulation, such as an anomalous anticyclone over the western North Pacific (WNP) and southerly anomalies over southeast China. While the climatological Atlantic SST is prescribed, the circulation over the WNP displays a significantly different pattern, with an eastward migration of the WNP anticyclone and the associated northerly anomalies over southeast China. It is argued that anticyclonic shear and Ekman divergence associated with the atmospheric Kelvin wave response to the TNA warm SSTA forcing is the primary mechanism for the generation of the anomalous anticyclone in WNP. The results presented in this study provide a teleconnection pattern between TNA and short-term climate variability in IEAM region.

ENSO, Indian monsoon, East Asian monsoon, western North Pacific anticyclone, Atlantic

Citation: Rong X Y, Zhang R H, Li T. Impacts of Atlantic sea surface temperature anomalies on Indo-East Asian summer monsoon-ENSO relationship. Chinese Sci Bull, 2010, 55: 2458–2468, doi: 10.1007/s11434-010-3098-3

The El Niño-Southern Oscillation (ENSO) is the most pronounced climate signal on the interannual timescale. As a coupled air-sea phenomenon of the tropical Pacific climate system, ENSO exhibits significant influences on the tropical and global climate. During ENSO episodes, anomalous sea surface temperature (SST) appears in the central-eastern equatorial Pacific. The SST anomaly (SSTA), on the one hand, directly induces climate variations over the extra-tropical Pacific through atmospheric teleconnection. On the other hand, it may exert a memory into other ocean basins through the "atmospheric bridge" [1,2], resulting in a long-persisting influence on the global climate even after ENSO has decayed.

*Corresponding author (email: rongur@cams.cma.gov.cn)

The connection between ENSO and the rainfall of China was long recognized by the Chinese researchers. Huang and Wu [3] found that in the developing summer of an El Niño, floods occur in the area from the Yangtze River valley to the Huaihe River valley, while droughts appear in the middle Yangtze River valley and North China. On the contrary, during the decaying summer, droughts may appear in the area from the Yangtze River valley to the Huaihe River valley. Liu and Ding [4] found that deficient rainfall tends to occur in the large part of China in the developing year of an El Niño, while in the subsequent year an opposite anomaly generally appears. Zhang et al. [5,6] pointed out that significant rainfall anomalies occur over South China during the autumn, winter and spring of the El Niño peak phase. The distinct characteristics of Chinese precipitation in the

different stages of ENSO are closely related to the anomalous atmospheric circulation in East Asia. Zhang et al. [7] revealed that an anomalous anticyclone over the Philippine Sea and western North Pacific (WNP) in the ENSO peak phase, which is the direct atmospheric Rossby wave response to the weakening of convection heating in WNP, is the major factor that causes the climate variation in the East Asia. Wang et al. [8,9] and Lau et al. [10] suggested that this anticyclone may be maintained from the El Niño mature winter to late spring through a positive local air-sea feedback. As a result of this positive feedback, a cold SSTA co-exists in WNP from the winter to late spring. Although the local positive air-sea feedback is not valid in the El Niño decaying summer (due to the change of the seasonal mean flow), the local cold SSTA may still partially contribute to the weakening of the WNP monsoon and the persistence of the anticyclone. The Indian Ocean (IO) may further act as a "capacitor" to maintain the anticyclone throughout the El Niño decaying summer [11,12].

So far, few works have been done to reveal the role of the Atlantic SSTA in the East Asian monsoon and the climate in China. Using an atmospheric general circulation model (AGCM), Lu et al. [13] showed that the simulated Indian and WNP monsoon circulation in 1998 becomes more consistent with the observation when the Atlantic SSTA effect is considered. Kucharski et al. [14] suggested that the decadal change of the ENSO-tropical Atlantic SST relationship after the 1980s causes the decrease of correlation between ENSO and Indian monsoon. Chen et al. [15] showed that the first EOF mode of the summer precipitation in China is closely related to the tropical North Atlantic (TNA) SSTA. Similar to the IO, a warm SSTA also appears in the TNA during the El Niño decaying year [16–18]. Does the TNA SSTA modulate the ENSO impact on the Indo-East Asian summer monsoon? What mechanism is responsible for this impact? The answer for these questions may advance our current understanding of the ENSO-monsoon relationship.

Due to the difficulty in simulating the observed anticorrelation between SST and rainfall in the monsoon region, the current state-of-the-art AGCMs generally have less skills in predicting the Asian-Pacific summer monsoon rainfall when forced by the observed SST [19–21]. Moreover, it is difficult to separate the pure effect of each basin as the SST in an individual basin may impact and be affected by other basins. In this study, we first explore the connection of the TNA SST variation to ENSO and the circulation over the Indo-East Asian monsoon (IEAM) region from a pure observational point of view. Then, a series of numerical experiments were conducted with a coupled atmosphere-ocean general circulation model. By allowing or prohibiting air-sea coupling in different basins, we intend to clarify the role of the Atlantic Ocean in modulating the ENSO-monsoon relationship.

1 Data and methods

The dataset used in the present study consists of (1) monthly SST from OISST [22] and HadISST [23] data sets, (2) air-sea flux data of OAFlux [24], (3) NCEP/NCAR reanalysis [25] 850 hPa wind data from 1979–2007, and (4) precipitation data of the Climate Prediction Center (CPC) Merged Analysis of Precipitation (CMAP) from 1979–2007 [26]. The SST data are the combination of the OISST dataset from 1982–2007 and the HadISST dataset from 1972–1981. The OAFlux heat flux data include the surface sensible and latent heat fluxes from 1981–2001, and the net short wave and long wave radiation fluxes from 1983–2001. In the following regression analysis between the Niño3 index (averaged SSTA over 150°W–90°W, 5°S–5°N) and heat flux/wind anomalies, the analysis period is based on that of the heat flux and wind fields respectively.

The model used in this study is a coupled version of the Max-Planck-Institute for Meteorology (MPI) ECHAM4 and the Geophysical Fluid Dynamics Laboratory (GFDL) MOM2 [27]. We used a T42 resolution for ECHAM4, with 19 vertical levels extending from the surface to 10 hPa. The ECHAM4 model has been documented in detail by Roeckner et al. [28]. The zonal resolution of MOM2 model is 2° and the meridional resolution varies from 0.5° within the equatorial band of 10°S–10°N to 2° poleward of 20°S(N). There are 30 unequal vertical levels with 22 levels in the upper ocean above 500 m. The PP scheme [29] is used for the vertical mixing. An anisotropic viscosity scheme similar to that of Large et al. [30] is adopted for horizontal viscosity. The ocean model is driven by the wind stress, heat flux and fresh water, and the atmosphere model is forced by the SST and surface currents predicted by the ocean model. The coupling interval is one day. The air-sea flux is calculated in the atmospheric model grid and is then interpolated through a conserved method into the oceanic model grid.

2 Observed relationships between the TNA SST and the Indo-East Asian monsoon anomalies

Figure 1(a) illustrates the correlation coefficients between the winter (November–January, NDJ0) Niño3 index and the subsequent summer (June–August, JJA1) SST and 850 hPa wind, calculated by the observed data. Here we define winter as November–January since ENSO generally peaks at December. It is seen that in the El Niño decayed summer, an anomalous anticyclone appears over the South China Sea (SCS) and WNP, and anomalous southerlies occur in the southeast and coastal areas of China. Easterly anomalies occur over the Bay of Bengal and the Arabian Sea. While warm SST anomalies appear in the northern IO and SCS, a cold SSTA appears in WNP, which is located to the east of the anomalous anticyclone. During the El Niño decaying summer, the SSTA in the eastern equatorial Pacific has

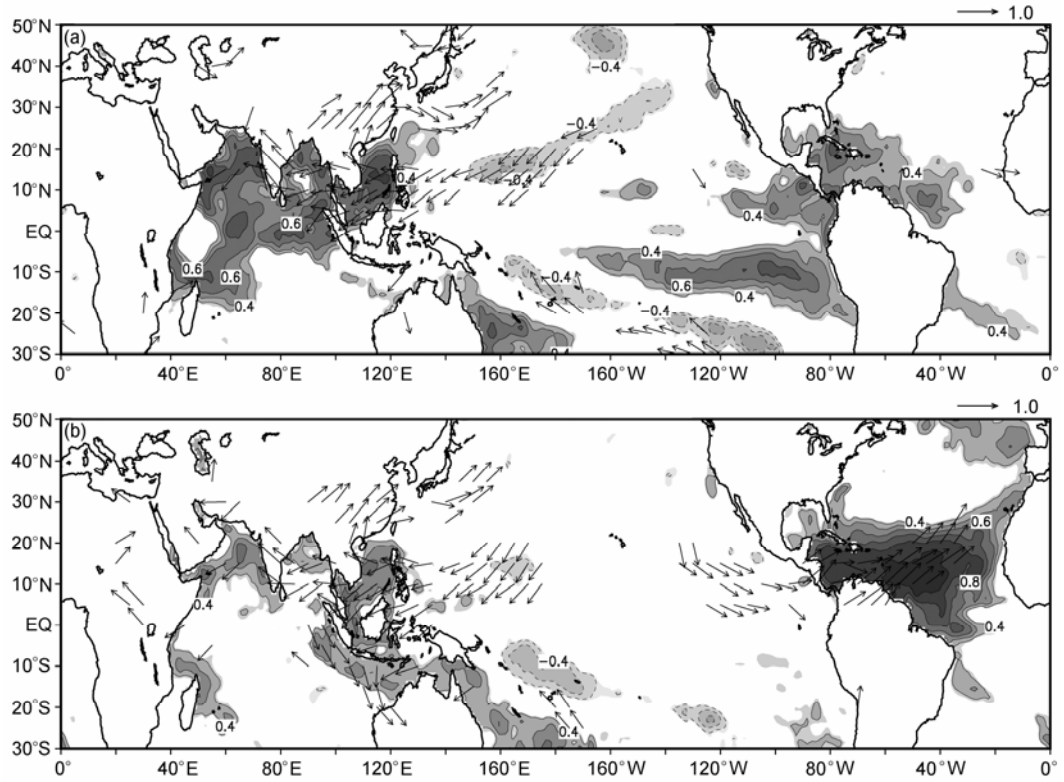

Figure 1 (a) Correlation between the winter Niño3 index (NDJ0) and the following summer (JJA1) SST (shaded) and 850 hPa wind (vector) anomalies; (b) simultaneous correlation between the JJA TATLI index and the SST and 850 hPa wind anomalies. Significant levels above 95% are shown.

rapidly decayed, so that significant SSTA signals are only found off the equator around 10°S(N). Note that a significant warm SSTA appears in the TNA from the equator to 20°N, but its horizontal extension and amplitude are relatively smaller compared to those in the IO.

A tropical Atlantic SST index (i.e., the TATLI index) is defined as the averaged SSTA over the TNA (80°–30°W, 0°–20°N). Figure 1(b) shows the simultaneous correlation between the JJA TATLI index and the SST/850 hPa wind anomalies. The correlation pattern of the wind field with the TATLI index over the IEAM region is quite similar to Figure 1(a). An anomalous anticyclone appears over the SCS and WNP, with southerly anomalies in the southeast China and easterly anomalies over the northern IO. We further calculated the partial correlation between the TATLI index and the 850 hPa wind (not shown), with the linear part related to the Niño3 index removed from both the TATLI index and the wind field. The result shows that the anticyclone still exists in the WNP and SCS, but the significant level is slightly reduced (still above 90%). This indicates that the SST in the TNA is closely related to the Asian monsoon circulation, but such a connection is largely modulated by ENSO.

In order to illustrate the relation between the TNA SSTA and ENSO, we calculated the lead-lag regression between the NDJ Niño3 index and the TATLI index (Figure 2). In Figure 2 the zero lag denotes December in the ENSO peak

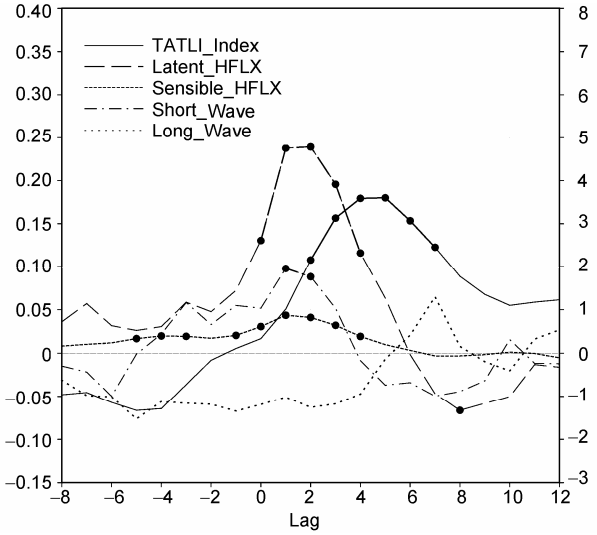

Figure 2 Lead-lag regression coefficients between the winter (NDJ) Niño3 index and the TATLI index (solid line, unit: °C °C^{-1}, left scale) and heat flux terms (unit: W m^{-2} °C^{-1}, right scale) anomalies averaged over 80°–30°W, 0°–20°N. The heat flux terms include: latent heat flux (long dashed line), sensible heat flux (short dashed line), net short wave (dot-dashed line) and long wave radiation (dot line). Positive lags denote the TATLI index/heat flux anomalies lag the Niño3 index by months. Significant levels above 95% are shown by heavy dots.

phase. It is seen that the TATLI index (solid line) is strongest when it lags the Niño3 index by 4 months, indicating that the TNA SSTA is most evident in the El Niño decaying

spring. The SSTA decreases gradually from the decaying spring to summer, but its significant level still exceeds 95% from June to July. The regressions of the surface latent and sensible heat fluxes and the long wave and short wave radiative fluxes are also shown in Figure 2. It is seen that the phases of these four heat fluxes lead the TATLI index about 2 months. During January-to-March when the SSTA rapidly grows, the sensible and latent heat fluxes and the short wave radiation all contribute positively to the SST growth (at 95% significant level). The greatest contribution comes from the latent heat flux, which is about twice as large as the short wave radiation and 5 times as large as the sensible heat flux. The long wave radiation tends to reduce the SSTA, but with a significant level less than 95%. The positive (negative) sensible and latent heat flux anomalies are ascribed to the anomalous westerly (easterly) over the TNA. From the El Niño mature winter to spring, the anomalous westerly over the TNA weakens the mean trade winds. The reduced wind speed decreases the upward latent and sensible heat fluxes and thus increases the SST. The anomalous westerly results from the teleconnection of the Atlantic atmosphere to the enhanced convective heating over the central-eastern equatorial Pacific. The increase of the downward short wave radiation is attributed to the anomalous Walker circulation. During El Niño episodes, the ascending branch displaces onto the central Pacific and descending motion occurs in the TNA, which reduces the cloud cover and thus increases the net solar radiation in the TNA. The short wave radiation anomaly becomes negative after the SSTA peaks, probably due to the local SSTA forcing effect. These results are in general consistent with the previous observational and AGCM studies [16–18].

The analysis above indicates that the TNA SSTA in boreal summer is closely related to the simultaneous Indo-East Asian monsoon and is greatly influenced by the preceding winter ENSO signals in the central-eastern Pacific. This provides an additional teleconnection mechanism through which ENSO impacts the Indo-East Asian summer monsoon. In the following sections, we investigate the specific process through which the Atlantic SSTA affects the ENSO-monsoon relationship through a series of numerical experiments.

3 Numerical experiments

3.1 Experimental design

In order to explore the impact of the Atlantic SSTA on the ENSO-monsoon relation, three sets of 16-member ensemble experiments were conducted, as listed in Table 1. In these experiments, the SST in the central-eastern Pacific (from 170°E to the coast of South America, 15°S–15°N) is prescribed from the observed monthly field during 1972–2007. Over this region, the SST in the ocean model is restored to the observational value with a Newtonian damping timescale of 5 days. In the control experiment (CTRL), the ocean and atmosphere are coupled everywhere except in the tropical central-eastern Pacific. The so-simulated ENSO-monsoon relation includes the impact of the SSTA from all ocean basins. In experiment CATLAN, climatological SST is used to force the atmosphere model in the Atlantic, where the ocean model is restored to the SST climatology. As the interannual variability of the Atlantic SST is excluded in CATLAN, by comparing this case with CTRL, one may reveal the impact of the Atlantic SSTA on the ENSO-monsoon relationship. In experiment CINDSCS the climatological SST is specified in the IO and SCS. This experiment is designed to examine the ENSO-monsoon relationship when only the air-sea coupling in the Pacific and Atlantic is considered. The model is integrated from 1972 to 2007, and the ensemble mean from 1979–2007 is used for the subsequent analysis.

To ensure that the mean states of the three experiments are same, an annual cycle flux correction method is applied to the SST field at each experiment. The numerical procedure is the following. First, the model was run for 50 years with a Newtonian damping term (at a damping timescale of 5 days) toward a prescribed SST climatological seasonal cycle. The last 20 years' Newtonian-damping terms were then averaged and used as the "flux correction" terms for the ocean model in the aforementioned experiments. These flux terms vary in space and with the seasonal cycle, and they only correct the model mean states but do not damp the model interannual variability. It was reported that due to the individual model errors, flux correction may distort the air-sea interactions and suppress the ENSO variability [31,32]. In the experiments mentioned above, observed SST is prescribed in the central-eastern Pacific, which guarantees the atmosphere model being forced by realistic ENSO signals and thus the atmosphere variability is not distorted by simulation errors of ENSO. The resulting simulations show that the model well keeps a realistic mean state, with the SST differences among three experiments less than 0.2°C in the IEAM region. It reproduces the observed anticorrelation relation between local SST and rainfall anomalies in the

Table 1 Experiments

Experiment	Central-eastern Pacific (east of 170°E, 15°S–15°N)	IO and SCS	Atlantic
CTRL	observation (1972–2007)	coupling	coupling
CATLAN	observation (1972–2007)	coupling	climatology
CINDSCS	observation (1972–2007)	climatology	coupling

monsoon region, the simultaneous negative ENSO-monsoon relation, and the teleconnection between ENSO and the global SST. Hence, the modeling results are more reliable with the use of the flux correction method.

3.2 Monsoon mean state and variability in the model

To examine the skill of the coupled model in simulating the monsoon mean state and variability, a 100-year run is performed. In this run the ocean and atmosphere are fully coupled everywhere. Figure 3(a) and (b) show the JJA precipitation and 850 hPa wind fields from observations and the coupled model simulation, respectively. Consistent with the simulation of Fu et al. [33], the unrealistic single rainbelt in the equatorial IO in a stand-alone ECHAM4 simulation is split into the northern rainbelt near 15°N and the equatorial rainbelt near 5°S in the coupled model. However, the intensity of the rainbelts in the coupled model is weaker than the observation. The rainfall center in SCS is also reproduced, but it shifts eastward onto the Philippines and its magnitude is largely reduced. The model failed to simulate the rainbelt in the western Pacific, and the maximum rainfall migrates onto the central Pacific. The model simulates well the tropical Atlantic rainfall pattern. The main features of the summer monsoon circulation such as the prominent zonal flows in the IO and the southwesterly flows over the southeast China are well reproduced. However, the simulated zonal velocity is somewhat weaker than the observed in the IO. In association with the eastward migration of the Pacific rainfall center, strong convergent flows appear around 160°W.

Figure 4(a) shows the standard deviation of SSTA derived from the 100-year simulation. Maximum SST variability locates in the eastern equatorial Pacific similar to the observation. The amplitude of the SST variability is a little weaker, compared to the observed. It is possible attributed to the relatively coarse resolution in the coastal region so that the model is unable to resolve the coastal upwelling along the coast of South America realistically. Figure 4(b) shows the simultaneous correlation between the DJF Niño3 index and the SST/850 hPa wind anomalies. The typical SST and circulation patterns during the El Niño mature phase, such as the pair of the anomalous anticyclone and the cold SSTA in the WNP, are reasonably reproduced. The results above indicate that the model used in the present study is able to capture the major features of the monsoon mean state and variability.

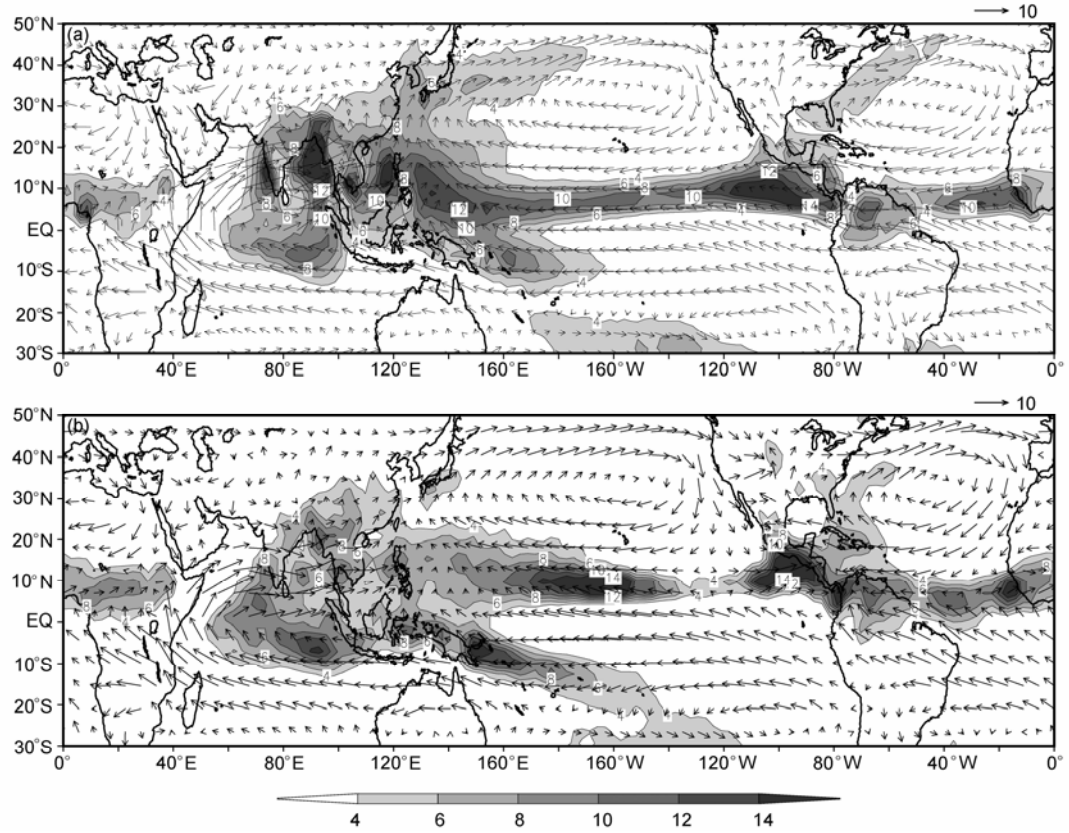

Figure 3 (a) Long-term mean JJA precipitation (shaded, unit: mm d^{-1}) and 850 hPa wind (vector, unit: m s^{-1}) from (a) observations; (b) 100-year simulation of the coupled model. The observed precipitation is derived from the CMAP data (1979–2007), and the 850 hPa wind from the NCEP/NCAR reanalysis (1979–2007).

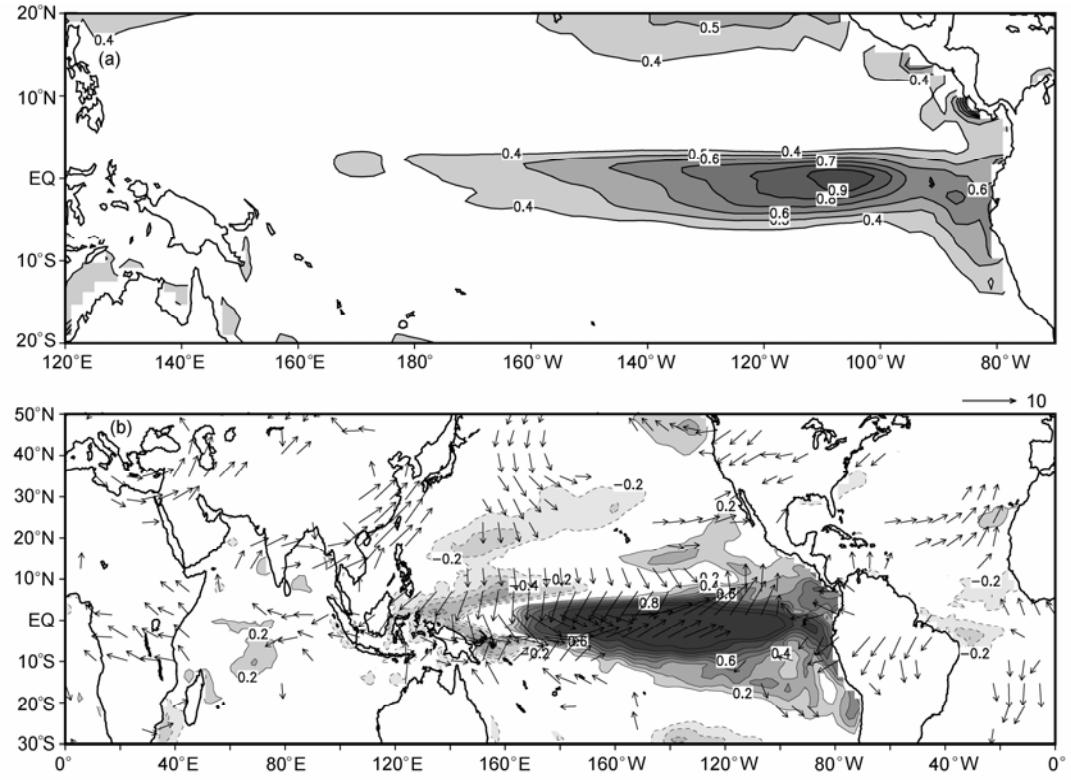

Figure 4 (a) Standard deviation of SSTA (unit: °C). (b) Simultaneous correlation between the DJF Niño3 index and the SST (shaded) and 850 hPa wind (vector) anomalies. (a) and (b) are derived from the couple model 100-year simulation.

3.3 ENSO-monsoon relationships under different air-sea coupling scenarios

Figure 5(a) illustrates the correlation between the NDJ0 Niño3 index and the JJA1 SST/850 hPa wind fields derived from the CTRL simulation. As revealed by observational studies, the summer SSTA in the tropical IO, SCS and Atlantic are positively correlated with the preceding winter Niño3 index, as a result of the teleconnection of the global ocean to ENSO through the "atmosphere bridge". The simulated correlation coefficients are larger than the observed when forced by the realistic ENSO SST signal, because the ensemble mean may greatly eliminate the influence of internal atmosphere variability and because the SST variation in other basins may largely reflect the impact of ENSO forcing. The WNP anticyclone anomaly is reasonably simulated in the CTRL simulation, although it is slightly shifted to the east compared to the observation. A cyclonic circulation anomaly appears over the eastern Pacific and Caribbean Sea, which is likely a Rossby wave response to the TNA warm SSTA forcing. A similar cyclonic circulation pattern exists in the observation (Figure 1(b)).

The simulation of experiment CATLAN is shown in Figure 5(b). The correlation pattern between the Niño3 index and 850 hPa wind field significantly changes when the Atlantic SSTA is excluded. Compared with CTRL, the correlation of the IO SST is weakened, implying that the Atlantic Ocean may enhance the basin-wide IO warming after the El Niño peak winter. Associated with the SST changes, the anticyclone anomaly in WNP moves further to the east. As a result, southeast China is dominated by northerly rather than southerly anomalies. Westerly anomalies appear in the northern IO, which is opposite to those in CTRL. The northerly in the southeast China is possibly associated with the cyclonic circulation in response to the warm SSTA in SCS. Anomalous westerlies appear from Africa to the western equatorial IO in response to the IO warming. The difference between CTRL and CATLAN implies that the persistence of the WNP anticyclone through the El Niño decaying summer depends not only on the local and IO SSTA forcing but also on the tropical Atlantic SSTA forcing.

Figure 5(c) shows the CINDSCS simulation result. When the SSTA in IO and SCS is not considered, the WNP wind pattern tends to resemble the CTRL simulation and the observation. Easterly anomalies are found over the equatorial and northern IO, extending westward onto Africa, which differs from experiment CATLAN. Anticyclonic circulations span from the WNP to the Bay of Bengal, inducing southerly anomalies in the southeast China and easterly anomalies in SCS and Bay of Bengal. The easterly anomalies reduce the mean summer monsoon to warm the local SST in the region. As a Rossby wave response to the Atlantic warm SSTA, cyclonic circulation appears near the Caribbean Sea and western TNA. It is more evident in CINDSCS

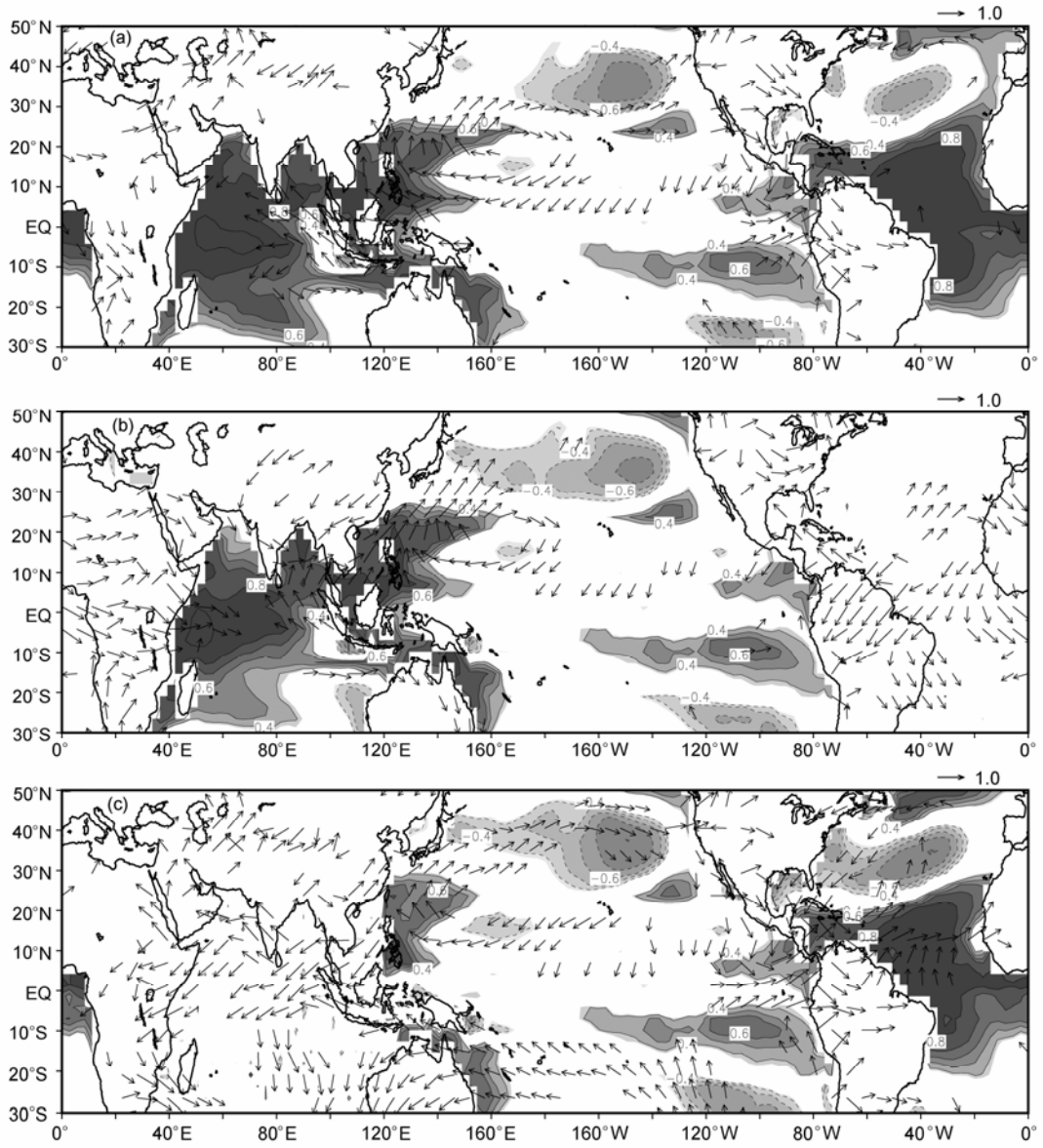

Figure 5 Correlation between the winter Niño3 index (NDJ0) and JJA1 SST (shaded) and 850 hPa wind (vector) anomalies derived from (a) CTRL simulation; (b) CATLAN simulation; (c) CINDSCS simulation. Significant levels above 95% are shown.

than in experiment CTRL. Since there is no SSTA forcing in the Indian Ocean and SCS, the anomalous circulation over the region is attributed to the SSTA in the Atlantic or Pacific.

The simulated lead-lag regression between the NDJ Niño3 index and the TATLI index is shown in Figure 6(a), derived from experiment CTRL. It is seen that the model result is quite consistent with the observation, except that the magnitude is somewhat larger. The SSTA in the TNA reaches maximum in the El Niño decaying spring, with the surface latent heat flux and short wave radiation contributing mostly to the SST tendency. The relative contribution of the surface net heat flux and 3D advection to the SSTA tendency is shown in Figure 6(b). Here a summer mean value (50 m) of the mixed layer depth is used. Note that the heat flux term is much larger than the advection term, indicating that the tropical Atlantic SSTA is primarily attributed to the heat flux anomaly in association with the atmospheric teleconnection to ENSO, whereas the ocean dynamics play a minor role. This result is consistent with the observational analysis [16] and mixed layer model simulations [2]. The zonal and vertical advections are in phase with the net heat flux term, while the meridional advection tends to reduce the SSTA. This is because the anomalous westerly in TNA may weaken the westward and upwelling flows, thus reducing the cold water advections and favoring a warm SSTA. The anomalous westerly may also weaken the poleward Ekman flow and decrease northward warm advection, leading to a cooling of SST there.

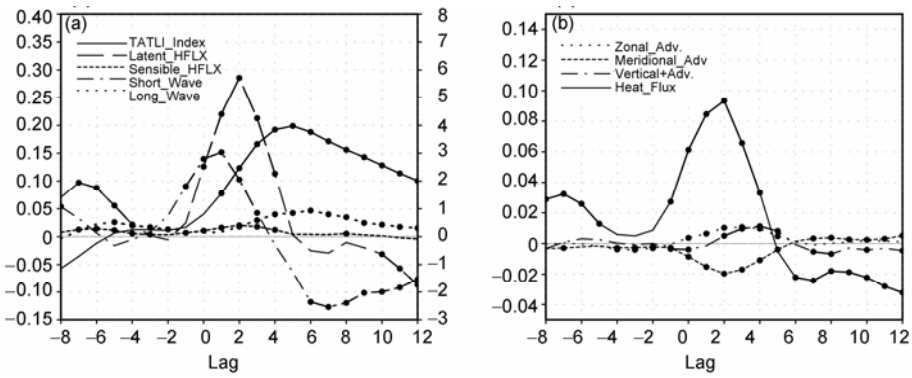

Figure 6 (a) Same as in Figure 2, but from the CTRL simulation. (b) Lead-lag regression coefficients between the NDJ Niño3 index and the heat flux tendency (solid line) and 3D advection averaged over 80°–30°W, 0°–20°N. Unit: °C month^{-1} °C^{-1}. Significant levels above 95% are shown by heavy dots.

4 Role of the Atlantic SSTA in inducing the Indo-Pacific circulation anomaly

To illuminate the mechanism through which the Atlantic SSTA affects the circulation anomaly in the IEAM region, we calculated the difference of regression coefficients between CTRL and CATLAN, as shown in Figure 7(a). From a linear thinking, the difference may be regarded as the sole contribution of the Atlantic SSTA. Note that the Atlantic SSTA induce not only the local circulation but also circulation anomalies over the tropical IO and WNP. While a cyclonic circulation anomaly appears to the west of the TNA heat source, striking easterly anomalies occur east of the heat source from Africa to the western Pacific. The easterly anomalies weaken the mean summer monsoon and thus increase the SST in the northern IO and SCS. This suggests that the Atlantic Ocean may partially contribute to the IO and SCS warming after the El Niño peak winter. The circulation anomalies over the East Asia and the Bay of Bengal resemble those in Figure 5(c). An anomalous anticyclone is clearly seen in the southeast China and WNP, indicating that the anticyclone in Figure 5(c) is primarily caused by the Atlantic SST anomalies.

It is worth mentioning that the IO warm SSTA alone may cause anomalous easterlies over the eastern IO and western Pacific and anomalous westerlies over Africa and the western IO. These westerlies, however, are offset by the easterlies produced by the Atlantic warm SSTA. As a result, there is no significant wind anomaly over the regions in CTRL. In the eastern IO and western Pacific, as will be discussed below, the anomalous easterlies caused by the IO SSTA are overlapped with those caused by the Atlantic SSTA. This favors the development of an anomalous anticyclonic circulation.

The Atlantic SSTA simulated by CTRL is greater than the observation. To demonstrate the realistic effect of the Atlantic SSTA, we performed an additional experiment (named OBSATL) in which the observed monthly SST (1972–2007) was used to force the atmosphere model in both the Atlantic and tropical central-eastern Pacific. Over other regions, the ocean and atmosphere were fully coupled. Figure 7(b) shows the difference of regression coefficients between OBSATL and CATLAN. The overall simulation pattern in OBSATL is quite similar to CTRL. Easterly anomalies are clearly presented over the equatorial and northern IO, and anomalous anticyclonic circulations occur over the WNP, SCS and the Bay of Bengal. This result demonstrates again the important role of the Atlantic SSTA on modulating the ENSO-monsoon relationship. The Atlantic Ocean may act as a delayed "bridge" to connect the winter ENSO signal and the subsequent summer monsoon circulation. The maximum easterly anomalies over the WNP in OBSATL shift further to the north compared to CTRL, because the observed Atlantic SSTA is primarily confined north of the equator while the SSTA in CTRL is more symmetric about the equator.

To reveal how the Atlantic SSTA impacts the Indo-East Asian monsoon circulation, we computed the simultaneous regression coefficients between the JJA TATLI index and the tropospheric temperature/850 hPa wind. Figure 8(a) shows the difference of regression coefficients between CTRL and CATLAN. As the TATLI index is highly correlated with the Niño3 index, the wind pattern in Figure 8(a) exhibits analogous features to Figure 7(a). The tropospheric temperature displays a typical Gill response pattern to the warm TNA SSTA, with a Kelvin wave response spanning from Africa to the western Pacific. Associated with the eastward extended warm tropospheric temperature, strong low-level easterly anomalies appear from IO to the tropical Pacific. Anomalous northeasterlies appear in the southern edge of the anticyclonic circulation, possibly caused by the Kelvin wave-induced Ekman divergence [12]. The negative shear vorticity caused by the Kevin wave-induced easterly suppresses the mean convection in the WNP monsoon region and thus induces anomalous anticyclonic circulation over there [12,34]. The numerical result suggests that the Atlantic may act as a "capacitor" analogous to IO in affecting the ENSO-monsoon relationship.

The difference between OBSATL and CATLAN is

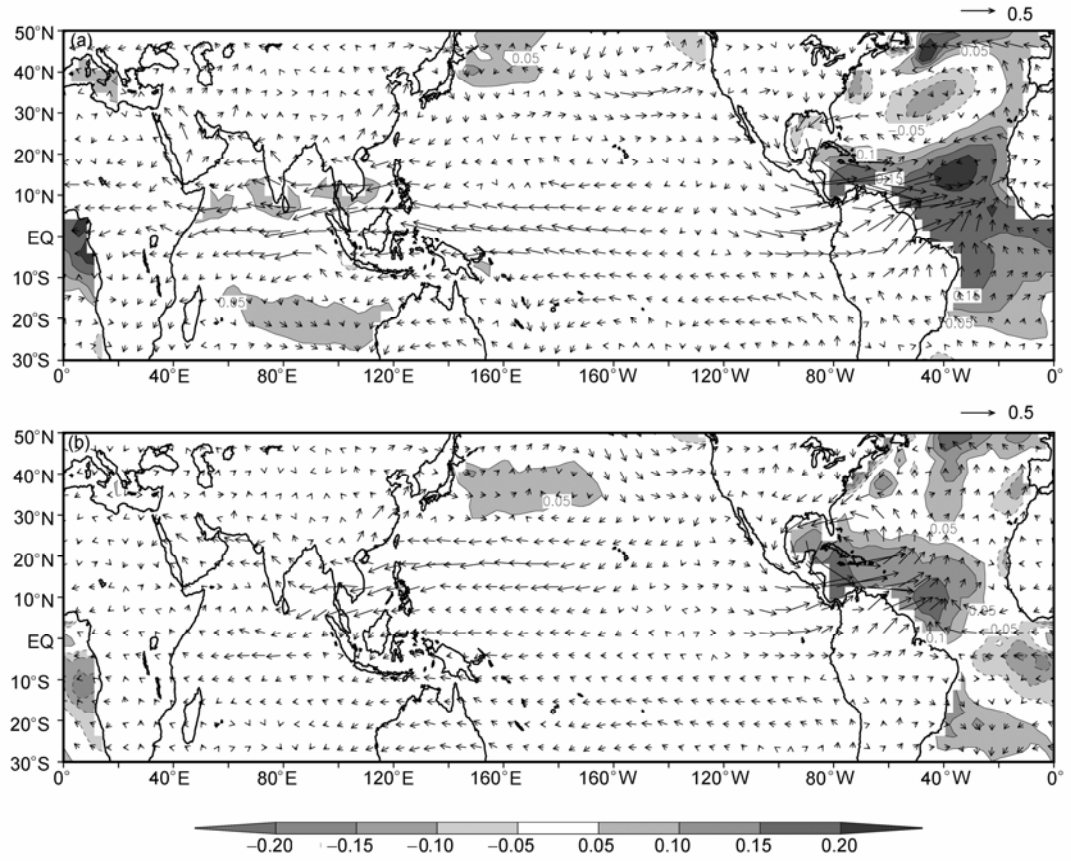

Figure 7 Difference of the regression coefficients between the winter (NDJ0) Niño3 index and the JJA1 SST (shaded, unit: °C °C^{-1}) and 850 hPa wind anomalies (vector, m s^{-1}°C^{-1}). (a) CTRL-CATLAN; (b) OBSATL-CATLAN.

shown in Figure 8(b). Similar features are found as in Figure 8(a). The anomalous easterlies dominate the area from Africa to the central equatorial Pacific. Warm tropospheric temperature anomalies extend eastward, displaying a Kelvin wave response pattern. Anomalous anticyclonic circulation appears in the Bay of Bengal and WNP. The results above confirm that the mechanism for the Atlantic SSTA to impact the Indo-East Asian monsoon is through the atmospheric Kelvin wave response.

5 Conclusions and discussion

The TNA SST bears a significant in-phase relationship with ENSO during the ENSO-decaying spring and summer. This in-phase relation primarily results from the surface latent heat flux and short wave radiation anomalies induced by the teleconnection of ENSO. The summer TNA SSTA exhibits a significant correlation with the simultaneous IEAM circulation, with a pattern analogous to the composite circulation anomaly during the ENSO-decaying summer. This suggests that the TNA SSTA may act as a "bridge" to link the winter ENSO to the subsequent summer monsoon circulation.

Numerical experiments reveal the importance of the TNA SSTA in inducing the IEAM circulation anomaly. When including air-sea coupling in the Atlantic, the model can reproduce the main characteristics of the IEAM circulation during the El Niño decaying summer, such as the WNP anticyclone and the corresponding southerly over the southeast and coastal area of China. While the climatological SST is prescribed in the Atlantic, the WNP anticyclone shifts to the east, with weakened easterly anomalies in the eastern IO and northerly anomalies in the southeast China associated with a cyclonic anomaly over the SCS. The simulated anomalous wind pattern is similar to the observed even when the SSTA in the IO and SCS is excluded. A further analysis shows that the Gill-type atmosphere response to the warm TNA SSTA produces Kelvin wave-induced easterly anomalies extending from the IO to the western Pacific. The anticyclonic shear associated with the easterly anomalies leads to the boundary layer divergence through Ekman pumping. The anomalous divergence further reduces the mean convection over the monsoon region, thus forming the anomalous anticyclonic circulation over the region.

We also conducted a stand-alone AGCM experiment by forcing ECHAM4 with the observed SSTA in the Atlantic (while the climatology SST is specified in other basins). The result shows that the observed warm SSTA in TNA

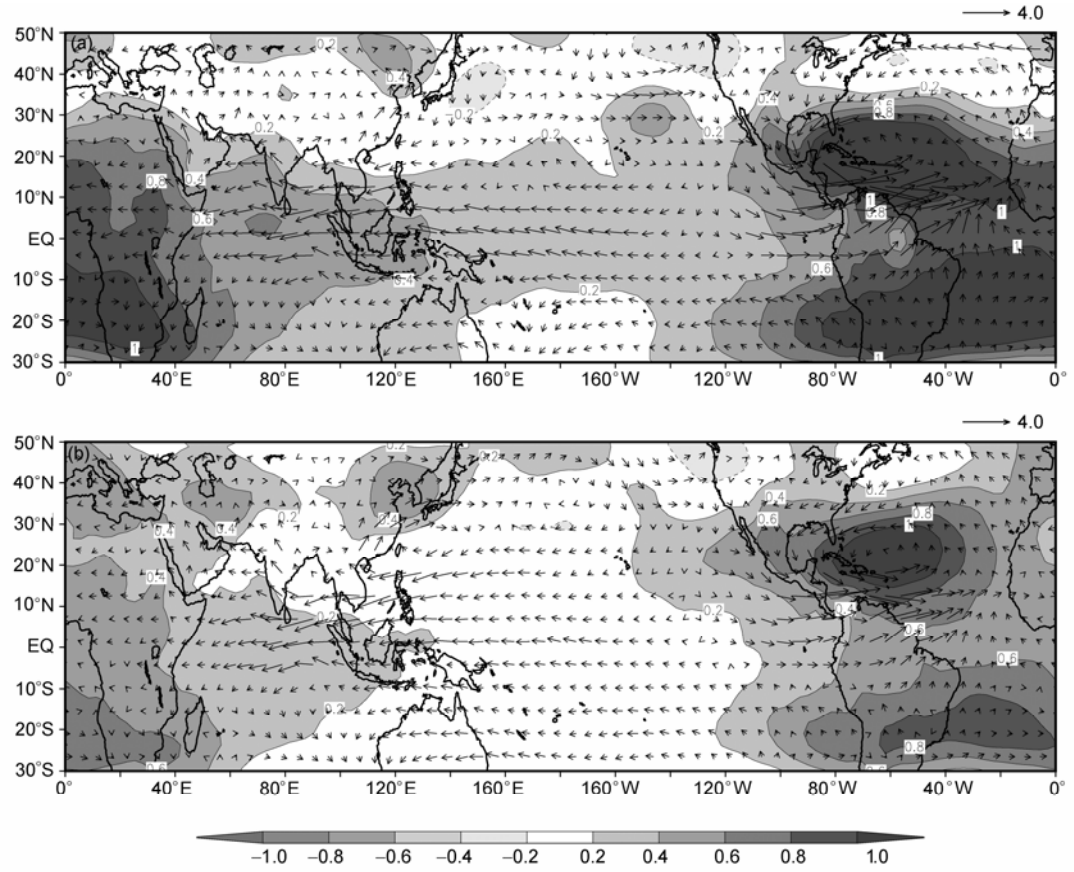

Figure 8 Difference of the simultaneous regression coefficients between the JJA TATLI index and the tropospheric temperature (200–850 hPa averaged, shaded, unit: °C °C^{-1}) and 850 hPa wind (vector, unit: °C °C^{-1}) anomalies. (a) CTRL-CATLAN; (b) OBSATL-CATLAN.

alone is able to generate an anticyclonic circulation pattern in WNP similar to that in the coupled model, even though the amplitude is slightly weaker. This indicates that the air-sea coupling may enhance the relationship between the TNA SSTA and the Asian monsoon, but the major mechanism responsible for the teleconnection is ascribed to the Kelvin wave response to the TNA SSTA.

As discussed by Xie et al. [12] and Wu et al. [34], the warm SSTA in IO may contribute to the persistence of the WNP anticyclone. The present study suggests that both the Atlantic and IO SSTA may contribute to the persistence of the WNP anticyclone throughout the El Niño decaying summer. The Atlantic Ocean may play an important role in "prolonging" the ENSO impact on the Indo-East Asian summer monsoon. Thus the TNA SSTA may be regarded as an additional predictand for the prediction of the interannual variability of circulation and precipitation anomalies in East Asia.

This work was supported by the National Basic Research Program of China (*2004CB418302*)*, the National Natural Science Foundation of China* (*40921003*) *and the International S&T Cooperation Project of the Ministry of Science and Technology of China* (*2009DFA21430*).

1 Lau N C, Nath M J. A modeling study of the relative roles of tropical and extratropical SST anomalies in the variability of the global atmosphere-ocean system. J Clim, 1994, 7: 1184–1207
2 Alexander M A, Bladé I, Newman M, et al. The atmospheric bridge: The influence of ENSO teleconnections on air-sea interaction over the global oceans. J Clim, 2002, 15: 2205–2231
3 Huang R H, Wu Y F. The influence of ENSO on the summer climate change in China and its mechanism. Adv Atmos Sci, 1989, 6: 21–32
4 Liu Y Q, Ding Y H. Reappraisal of the influence of ENSO events on seasonal precipitation and temperature in China (in Chinese). Sci Atmos Sin, 1995, 19: 200–208
5 Zhang R, Sumi A, Kimoto M. A diagnostic study of the impact of El Niño on the precipitation in China. Adv Atmos Sci, 1999, 16: 229–241
6 Zhang R, Sumi A. Moisture circulation over East Asia during El Niño episode in northern winter, spring and autumn. J Meteor Soc Jpn, 2002, 80: 213–227
7 Zhang R, Sumi A, Kimoto M. Impact of El Niño on the East Asian monsoon: A diagnostic study of the '86/87 and '91/92 events. J Meteor Soc Jpn, 1996, 74: 49–62
8 Wang B, Wu R, Fu X. Pacific-East Asia teleconnection: How does ENSO affect East Asian climate? J Clim, 2000, 13: 1517–1536
9 Wang B, Wu R, Li T. Atmosphere-warm ocean interaction and its impact on Asian-Australian monsoon variability. J Clim, 2003, 16: 1195–1211
10 Lau N C, Nath M J. Impact of ENSO on the variability of the Asian-Australian monsoons as simulated in GCM experiments. J Clim, 2000, 13: 4287–4309
11 Yang J L, Liu Q Y, Xie S P, et al. Impact of the Indian Ocean SST basin mode on the Asian summer monsoon. Geophys Res Lett, 2007, 34: L02708, doi:10.1029/2006GL028571

12 Xie S P, Hu K, Hafner J, et al. Indian Ocean capacitor effect on Indo-Western Pacific climate during the summer following El Niño. J Clim, 2009, 22: 730–747
13 Lu R, Dong B. Impact of Atlantic sea surface temperature anomalies on the summer climate in the western North Pacific during 1997–1998. J Geophys Res, 2005, 110: D16102, doi:10.1029/2004JD-005676
14 Kucharski F, Bracco A, Yoo J H, et al. Low-frequency variability of the Indian monsoon-ENSO relationship and the tropical Atlantic: The "weakening" of the 1980s and 1990s. J Clim, 2007, 20: 2255–2265
15 Chen W, Kang L H, Wang D. The coupling relationship between summer rainfall in China and global sea surface temperature (in Chinese). Clim Environ Res, 2006, 11: 259–269
16 Klein S A, Soden B J, Lau N C. Remote sea surface variations during ENSO: Evidence for a tropical atmospheric bridge. J Clim, 1999, 12: 917–932
17 Saravanan R, Chang P. Interaction between tropical Atlantic variability and El Niño-Southern Oscillation. J Clim 2000, 13: 2177–2194
18 Giannini A, Kushnir Y, Cane M A. Interannual variability of Caribbean rainfall, ENSO and the Atlantic Ocean. J Clim, 2000, 13: 297–311
19 Wang B, Kang I S, Lee J Y. Ensemble simulations of Asian-Australian monsoon variability by 11 AGCMs. J Clim, 2004, 17: 803–818
20 Wang B, Ding Q H, Fu X H, et al. Fundamental challenge in simulation and prediction of summer monsoon rainfall. Geophys Res Lett, 2005, 32: L15711, doi: 10.1029/2005GL022734
21 Wu B, Zhou T, Li T. Contrast of rainfall-SST relationships in the western north Pacific between the ENSO-developing and ENSO-decaying summers. J Clim, 2009, 22: 4398–4405
22 Reynolds R W, Rayner N A, Smith T M, et al. An improved *in situ* and satellite SST analysis for climate. J Clim, 2002, 15: 1609–1625
23 Rayner N A, Horton E B, Parker D E, et al. Version 2.2 of the Global sea-ice and Sea Surface Temperature data set, 1903–1994. Clim Res Tech Note 74, 1996
24 Yu L, Jin X, Weller V. Multidecade Global Flux Datasets from the Objectively Analyzed Air-sea Fluxes (OAFlux) Project: Latent and sensible heat fluxes, ocean evaporation, and related surface meteorological variables. Woods Hole Oceanographic Institution OAFlux Project Technical Report, 2008
25 Kalnay E, Kanamitsu M, Kistler M. The NCEP/NCAR 40-year reanalysis project. Bull Am Meteorol Soc, 1996, 77: 437–471
26 Xie P, Arkin P A. Global precipitation: A 17-year monthly analysis based on gauge observations, satellite estimates, and numerical model outputs. Bull Am Meteorol Soc, 1997, 78: 2539–2558
27 Pacanowski R C. MOM2 Documentation, user's guide and reference manual. GFDL Ocean Technical Report 3.2., 1996
28 Roeckner E, Arpe K, Bengtsson L. The atmospheric general circulation model ECHAM-4: Model description and simulation of present-day climate. Max-Planck-Institute for Meteorology Report 218, 1996
29 Pacanowski R C, Philander G. Parameterization of vertical mixing in numerical models of the tropical ocean. J Phys Oceanogr, 1981, 11: 1442–1451
30 Large W G, Danasbogulu G, McWilliams J C, et al. Equatorial circulation of a global ocean climate model with anisotropic viscosity. J Phys Oceanogr, 2001, 31: 518–536
31 Neelin J D, Dukstra H A. Ocean-atmosphere interaction and the tropical climatology. Part I: The dangers of flux correction. J Clim, 1995, 8: 1325–1342
32 Latif M, Sterl A, Maier-Reimer E, et al. Climate variability in a coupled GCM. Part I: The tropical Pacific. J Clim, 1993, 6: 5–21
33 Fu X, Wang B, Li T. Impacts of air-sea coupling on the simulation of mean Asian summer monsoon in the ECHAM4 model. J Clim, 2002, 15: 2889–2904
34 Wu B, Zhou T, Li T. Seasonally evolving dominant interannual variability modes of East Asian Climate. J Clim, 2009, 22: 2992–3005